PNAS RESEARCH ARTICLE | DEVELOPMENTAL BIOLOGY

A highly reproducible and efficient method for retinal organoid differentiation from human pluripotent stem cells

Jade Harkin[a,b], Kiersten H. Peña[b,c], Cátia Gomes[b,d], Melody Hernandez[b,d], Sailee S. Lavekar[b,c], Kaman So[d], Kelly Lentsch[b,c], Elyse M. Feder[b,e], Sarah Morrow[b], Kang-Chieh Huang[b,c], Kaylee D. Tutrow[b,d], Ann Morris[f], Chi Zhang[d], and Jason S. Meyer[a,b,d,g,1]

Affiliations are included on p. 11.

Edited by Robert Johnston, Johns Hopkins University, Baltimore, MD; received October 9, 2023; accepted May 15, 2024 by Editorial Board Member Jeremy Nathans

Human pluripotent stem cell (hPSC)-derived retinal organoids are three-dimensional cellular aggregates that differentiate and self-organize to closely mimic the spatial and temporal patterning of the developing human retina. Retinal organoid models serve as reliable tools for studying human retinogenesis, yet limitations in the efficiency and reproducibility of current retinal organoid differentiation protocols have reduced the use of these models for more high-throughput applications such as disease modeling and drug screening. To address these shortcomings, the current study aimed to standardize prior differentiation protocols to yield a highly reproducible and efficient method for generating retinal organoids. Results demonstrated that through regulation of organoid size and shape using quick reaggregation methods, retinal organoids were highly reproducible compared to more traditional methods. Additionally, the timed activation of BMP signaling within developing cells generated pure populations of retinal organoids at 100% efficiency from multiple widely used cell lines, with the default forebrain fate resulting from the inhibition of BMP signaling. Furthermore, given the ability to direct retinal or forebrain fates at complete purity, mRNA-seq analyses were then utilized to identify some of the earliest transcriptional changes that occur during the specification of these two lineages from a common progenitor. These improved methods also yielded retinal organoids with expedited differentiation timelines when compared to traditional methods. Taken together, the results of this study demonstrate the development of a highly reproducible and minimally variable method for generating retinal organoids suitable for analyzing the earliest stages of human retinal cell fate specification.

organoid | stem cell | retina

Significance

Retinal organoids are retinal-like tissues derived from human pluripotent stem cells (hPSCs) that effectively recapitulate the major stages of human retinogenesis. Several protocols have been developed to generate retinal organoids in vitro, yet few protocols have focused on 1) maximizing the efficiency of retinal organoid generation, 2) enhancing the reproducibility of individual organoids, and 3) elucidating the mechanisms underlying the earliest stages of retinal organoid specification. In this study, through regulation of multiple parameters, we have generated a more highly standardized and efficient method to yield consistently pure populations of retinal organoids of consistent size and shape across multiple cell lines.

The differentiation of human pluripotent stem cells (hPSCs) into three-dimensional retinal organoids has enabled unprecedented access into the study of human retinogenesis (1–5), as well as analyses of retinal degenerative diseases from patient-derived sources (6–10). Through the differentiation of retinal organoids, hPSCs differentiate into primitive retinal-like tissue in a manner that closely mimics the spatial and temporal development and organization of the human retina (1, 5, 11–16). As such, retinal organoids have served as an effective in vitro model for the study of features underlying human retinogenesis, as well as a platform to elucidate mechanisms associated with retinal degenerative diseases. Other studies have also explored the use of retinal organoids for pharmacological screening (2, 17, 18), as well as for cellular replacement in retinal diseases (19–22), further underscoring the tremendous potential of retinal organoids for a variety of translational applications.

While current retinal organoid differentiation protocols have allowed for many advances in the study of human retinal development and disease (3, 5, 12, 15, 23–26), shortcomings in the efficiency and reproducibility of these protocols have hindered their use for some translational applications. Existing protocols have demonstrated a great deal of variability in the efficiency of retinal organoid production, including from one cell line to another as well as among individuals performing the differentiation (23, 27). Additionally, even when retinal organoids are effectively formed, they often exhibit broad variability in their size and shape, making direct comparisons across organoids and experiments exceedingly difficult, particularly for more high-throughput applications (15, 23, 25). Thus, a great need exists to refine current protocols to increase the efficiency of retinal organoid production, as well as to minimize the variability observed among retinal organoids produced.

To address these shortcomings, we have advanced existing retinal organoid differentiation protocols (5, 11, 12, 15) to generate 3D retinal organoids at 100% efficiency and with significantly greater reproducibility in their size, shape, and cellular composition,

Author contributions: J.H. and J.S.M. designed research; J.H., K.H.P., C.G., M.H., S.S.L., S.M., K.-C.H., K.D.T., and J.S.M. performed research; J.H., K.H.P., K.S., K.L., E.M.F., K.D.T., A.M., C.Z., and J.S.M. analyzed data; and J.H., M.H., and J.S.M. wrote the paper.

Competing interest statement: J.H. and J.S.M. have filed a patent related to the methodology described in this paper.

This article is a PNAS Direct Submission. R.J. is a guest editor invited by the Editorial Board.

[1]To whom correspondence may be addressed. Email: meyerjas@iu.edu.

This article contains supporting information online at https://www.pnas.org/lookup/suppl/doi:10.1073/pnas.2317285121/-/DCSupplemental.

Published June 13, 2024.

while also demonstrating the ability to completely block retinal specification through the modulation of BMP signaling. To demonstrate the robustness of these approaches, we analyzed the ability to derive retinal organoids across six different lines of hPSCs (*SI Appendix*, Table S1), including both human embryonic stem cells (hESCs) and human induced pluripotent stem cells (iPSCs). These lines also represented those from both male and female cell donors, as well as cell lines previously described to be either "good" or "bad" producers of retinal organoids. Given this ability to modulate retinal organoid differentiation on demand to yield 100% purity of retinal organoids or conversely to completely prevent retinal organoid specification, we explored the ability to assess the earliest stages of human retinogenesis via RNA-seq analyses, highlighting important transcriptional signatures associated with the initial specification of a retinal fate from a more primitive neuroepithelial population. Upon long-term differentiation using these more standardized methods, retinal organoids also displayed expedited retinal neuron differentiation timelines compared to organoids differentiated using traditional methods. Taken together, the results of this study provide a more standardized and efficient method for generating highly reproducible retinal organoids, greatly facilitating the study of human retinogenesis and providing essential improvements for future disease modeling and pharmacological screening applications.

Results

Enhancing the Reproducibility of Early-Stage Cellular Aggregates. Previous studies have demonstrated that individual retinal organoids are often highly variable based upon their size and shape, confounding the application of retinal organoids for a variety of downstream studies (13–15, 23, 27). We theorized that this high degree of variability among retinal organoids was due, at least in part, to a high degree of variability introduced into the system at the earliest stages of differentiation. Indeed, following traditional differentiation protocols for the production of retinal organoids, we observed a great range of variability in the size and shape of hPSC aggregates from the start of the differentiation process, which was evident within the first few days of differentiation (Fig. 1*A*). As traditional methods often rely upon the use of proteolytic enzymes such as dispase to release hPSC colonies intact to form cellular aggregates (5, 15), and the size and shape of these aggregates are dependent upon the size and shape of the original colony, we sought to determine whether we can minimize variability at these early stages. To overcome this variability, we sought to generate cellular aggregates of consistent size and shape through dissociation of hPSC colonies into single-cell suspensions. Subsequently, singularized cells were seeded into low-adhesion 96-well U-bottom plates at defined cell numbers followed by centrifugation resulting in a forced reaggregation, producing aggregates that were more consistent in both their size and shape (Fig. 1*B* and Movie S1). Fusion of cellular aggregates can also lead to variability in their size and shape, particularly at the earlier stages of differentiation. Therefore, to combat this we transferred approximately 45 to 48 cellular aggregates to each of two 10 cm dishes on Day 1 and gently agitated the plates to prevent fusion every 2 to 3 d. Next, to determine whether this enhanced reproducibility of early hPSC aggregates was dependent upon their starting size, we tested a range of different cell densities (250, 500, 1,000, 2,000, 4,000, and 8,000) cells per well (cpw) and quantified the two-dimensional area and circularity at Day 3 and Day 6 when differentiated using the standardized method compared to those grown via traditional methods (Fig. 1 *J–O*). We observed that while cellular aggregates grown via the traditional method exhibited a range of sizes and shapes, cellular aggregates grown via standardized methods at all seeding densities were much more highly reproducible among individual aggregates at both Day 3 (Fig. 1 *J–L*) and Day 6 of retinal organoid differentiation (Fig. 1 *M–O*).

As the above experiments were initially conducted with the H7 human embryonic stem cell line, we then sought to test whether these initial improvements in aggregate reproducibility could be similarly replicated across other hPSC lines. To further test the reproducibility of the standardized method, we selected two additional hPSC lines, including the H9 embryonic stem cell line as well as the PGP1 induced pluripotent stem cell line (*SI Appendix*, Table S1). These cell lines were then subjected to the same differentiation conditions and quantified as described above, with each of these additional cell lines demonstrating a very similar trend for greater reproducibility of the size and shape of cellular aggregates at both Day 3 and Day 6 of differentiation (*SI Appendix*, Fig. S1), demonstrating the ability to minimize variability across a variety of cell lines, providing a more level starting point for subsequent retinal organoid differentiation.

Establishing an Appropriate Number of Cells Per Aggregate to Optimize Retinal Specification. Next, we wanted to explore whether the size of initial hPSC aggregates had any influence upon their ability to effectively give rise to retinal lineage cell populations. To achieve this, we leveraged a recently described SIX6:GFP reporter cell line as an indicator of effective retinal fate specification (28). As SIX6 is perhaps the earliest retinal lineage-specific transcription factor (5, 28, 29), the expression of GFP would indicate the earliest stages of retinal fate determination. Similar to the approaches described above, hPSCs were enzymatically dissociated into a single-cell suspension and reaggregated into aggregates of defined sizes, from 250 to 8,000 cpw (Fig. 2*A*). These aggregates were then differentiated according to defined retinal organoid differentiation protocols and assessed for the acquisition of a retinal fate based upon the expression of the SIX6:GFP reporter (Fig. 2). While GFP-positive retinal cells were identified in all experimental conditions, it was noteworthy that lower cellular densities (e.g., 250 and 500 cells per well) yielded a reduced capacity for retinal differentiation (Fig. 2 *B–H*). Conversely, we reproducibly achieved 100% efficiency of retinal lineage specification when the initial aggregate size was established between 1,000 cells per well to 8,000 cells per well (Fig. 2 *B* and *I–T*), with all aggregates robustly expressing the SIX6-GFP reporter. Once we established that 1,000 cells per well to 8,000 cells per well generated pure populations or retinal organoids, we decided to use a seeding density of 2,000 cells/aggregate for further experiments, as this density appeared to provide the greatest reproducibility of early cellular aggregates (Fig. 1) as well as 100% efficiency of retinal fate specification (Fig. 2). To determine how many of the original 96 cellular aggregates per plate were conserved throughout differentiation, we then differentiated cellular aggregates using the standardized method and quantified the total number of cellular aggregates at Day 1 (after transferring from the 96-well plates), Day 8 (before plating), Day 16 (before lifting), and Day 20 (when a vesicle-like morphology can be identified), with these studies demonstrating that a large majority of initial cellular aggregates were retained throughout the differentiation process, and most loss of organoids was observed after lifting organoids on Day 16 (*SI Appendix*, Fig. S2). Taken together, these results overall demonstrated an important dependency of initial aggregate size upon their ability to effectively differentiate along the retinal lineage, providing promising opportunities for future studies of human retinogenesis and how tissue size may regulate retinal specification.

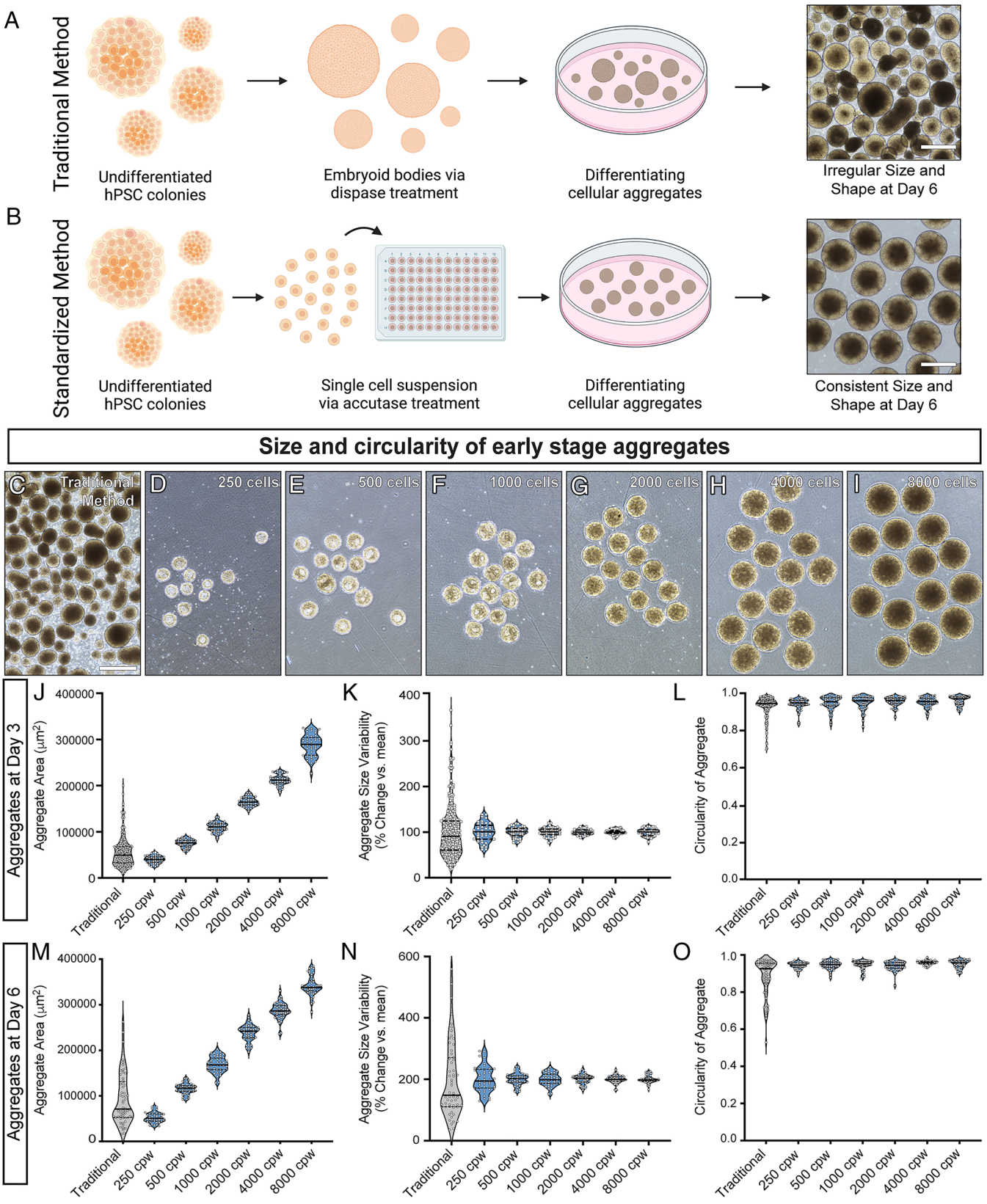

Fig. 1. Reproducibility of early-stage cellular aggregates. (*A* and *B*) Schematic of traditional and standardized methods of differentiation. The schematic shows representative images of cellular aggregates differentiated until Day 6 using the traditional and standardized methods. (*C*) Representative images of cellular aggregates differentiated until Day 3 using the traditional method. (*D–I*) Representative images of cellular aggregates at different densities (250, 500, 1,000, 2,000, 4,000, and 8,000 cells per well) differentiated until Day 3 using the standardized method. (*J–O*) Compared to the traditional method, the standardized method is highly reproducible generating cellular aggregates that are more consistent in both their size and circularity at both Day 3 and Day 6. (Scale bars equal 500 μm (*A–C*).) The scale bar in (*C*) applies to (*D–I*). n = 3 biological replicates for each cell line.

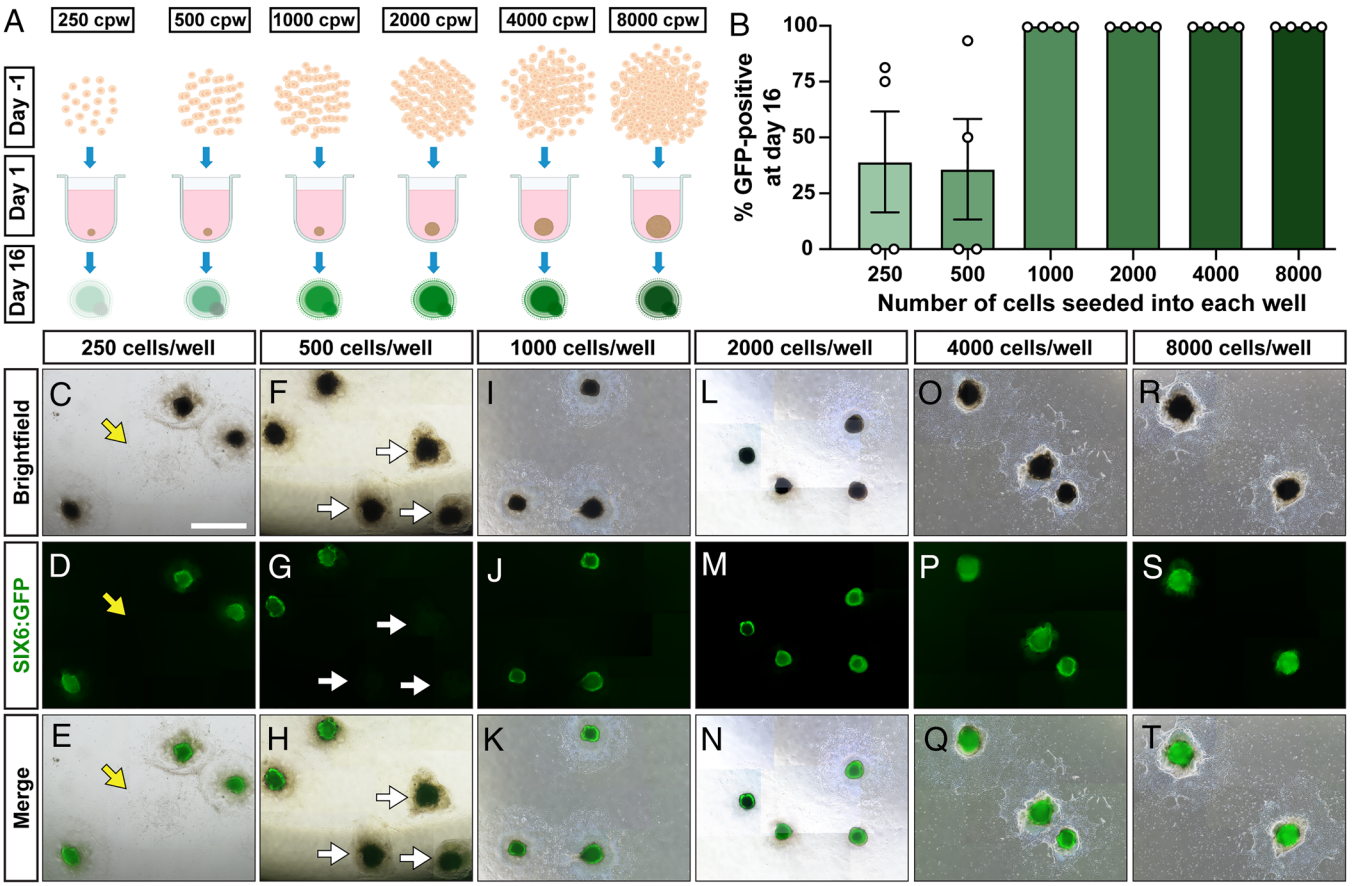

Fig. 2. Establishing the appropriate cell density for efficient retinal organoid formation. (*A*) Schematic demonstrating the process of establishing standardized cellular aggregates of defined cell densities for the subsequent differentiation of retinal organoids. (*B*) Quantification of retinal organoid differentiation efficiency based upon the size of original cell aggregates at Day 16, as determined by the expression of a SIX6:GFP reporter (n = 4 biological replicates). (*C*–*T*) Representative images at Day 16 by brightfield microscopy, fluorescence microscopy for SIX6:GFP expression, as well as merged images for each starting cell density. The yellow arrowhead indicates an aggregate that flattened out and failed to differentiate into retinal lineage. White arrowheads indicate aggregates that remained three-dimensional but did not differentiate into retinal lineage. The scale bar equals 1,000 μm.

Improved Efficiency and Reproducibility of Retinal Organoids Produced by Standardized Methods. With the ability to greatly reduce variability in early hPSC aggregates at the start of the differentiation process (Fig. 1), as well as the finding that initial aggregate size played an important role in the ability of aggregates to achieve a retinal fate (Fig. 2), we next sought to determine whether this improved reproducibility translated into any improvements in the variability of subsequently differentiated retinal organoids. To explore this possibility, we similarly used the IMR90-4 SIX6-GFP reporter cell line. Retinal organoids were differentiated by either traditional methods (TM) or standardized methods (SM) using an initial seeding density of 2,000 cells/aggregate and cells were directed to differentiate into retinal organoids until a total of 25 d of differentiation. Using the expression of the SIX6:GFP as a specific retinal progenitor marker, we then sought to quantify the percentage of cellular aggregates that effectively differentiated into retinal organoids based on GFP expression. As previous studies have also shown that the precise timing of BMP4 treatment can enhance retinal organoid production (23, 30), we also tested a role for BMP4 signaling at early stages of retinal specification by treating cellular aggregates at Day 6 with either BMP4 (50 ng/mL) or the small molecule BMP inhibitor LDN-193189 (200 nM). Accordingly, when organoids were differentiated using the traditional method without BMP4 treatment, approximately 38.67% ± 6.12% (SEM) of organoids expressed the SIX6:GFP reporter (Fig. 3 *A*, *B*, and *M*). When early cellular aggregates differentiated using the traditional method and exposed to BMP4 at Day 6, the efficiency of retinal organoid differentiation increased to 84.33% ± 2.91% based on GFP expression (Fig. 3 *C*, *D*, and *M*). Next, we applied similar differentiation strategies to cellular aggregates generated using the standardized method of differentiation. When organoids were differentiated using the standardized method without BMP4 treatment, approximately 51.67% ± 20.93% of organoids expressed the SIX6:GFP reporter (Fig. 3 *E*, *F*, and *M*). However, when aggregates were differentiated using the standardized method combined with BMP4 treatment at Day 6, the efficiency of retinal organoid production was enhanced to 100% in all experiments based on SIX6:GFP expression (Fig. 3 *G*, *H*, and *M*). Conversely, when BMP4 signaling was blocked using the small molecule BMP inhibitor LDN-193189, organoids differentiated using both the traditional and standardized method lacked any expression of the SIX6:GFP reporter (Fig. 3 *I*–*M*), demonstrating a necessity for BMP signaling in retinal specification. Interestingly, organoids that failed to adopt a retinal phenotype were found to exclusively adopt a cortical forebrain phenotype, based upon the expression of markers such as FOXG1 and CTIP2 (*SI Appendix*, Fig. S3). In addition to the purity of retinal organoid differentiation through the use of the standardized method along with BMP4 exposure, we also sought to determine whether the standardized method also enhanced the reproducibility of individual retinal organoid size and shape. By quantifying the two-dimensional area and circularity of differentiated retinal organoids, we found that the standardized method was not only more efficient at generating retinal organoids but also produced more highly reproducible organoids based upon a more consistent size and circularity at Day

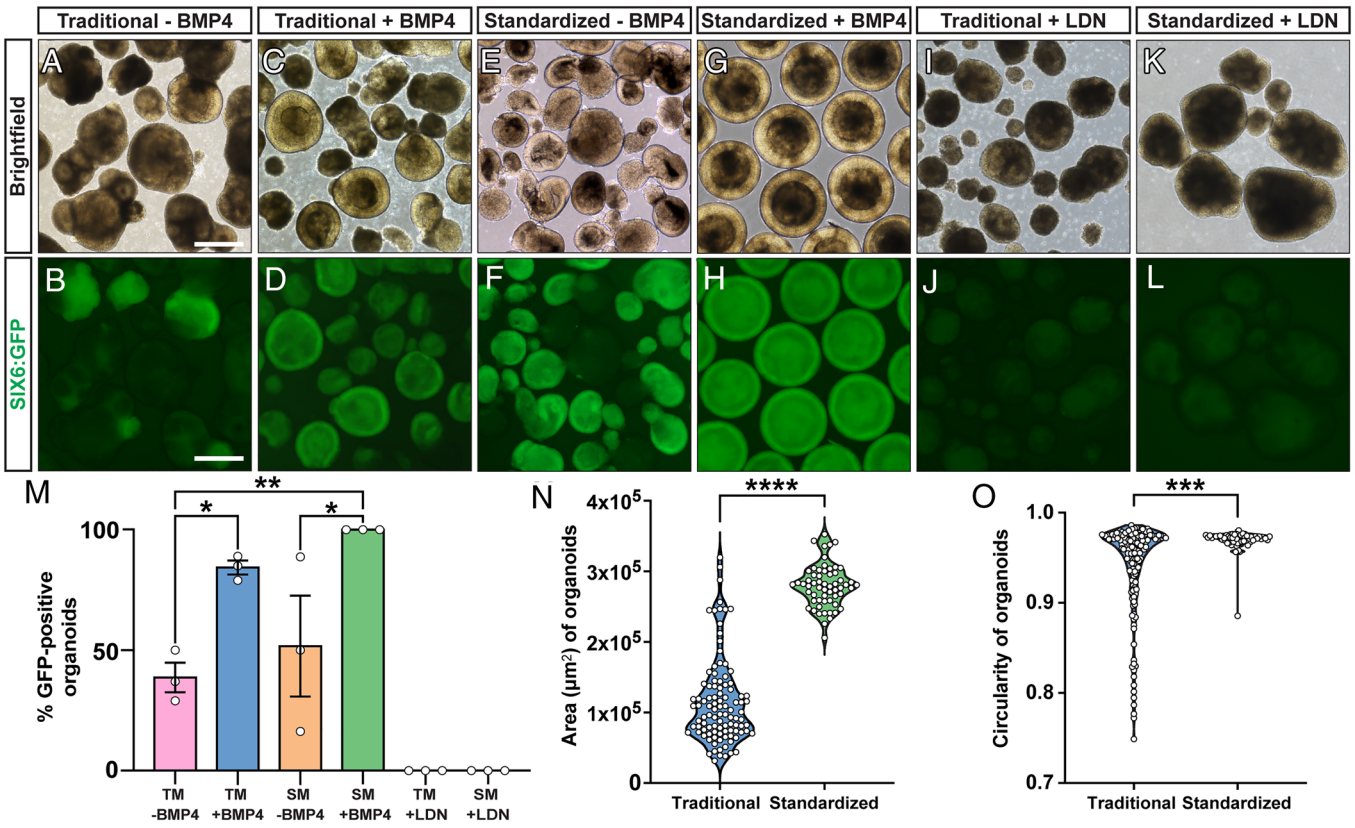

Fig. 3. Highly efficient differentiation of retinal organoids via standardized methods. (*A*–*L*) Brightfield and fluorescent images of organoids at Day 25 differentiated using the SIX6-GFP reporter cell line by either the traditional method or the standardized method. (*A*, *B*, and *M*) Organoids differentiated using the traditional method without BMP4 treatment generated retinal organoids at an efficiency of 38.67% ± 6.12% expressing the SIX6:GFP reporter. (*C*, *D*, and *M*) Organoids differentiated using the traditional method with BMP4 supplementation improved the efficiency of retinal organoid differentiation to 84.33% ± 2.91% of organoids expressing SIX6-GFP. (*E*, *F*, and *M*) Organoids differentiated using the standardized method without BMP4 treatment generated approximately 51.67% ± 20.93% (SEM) of organoids that express the SIX6:GFP reporter. (*G*, *H*, and *M*) Organoids differentiated using the standardized method with BMP4 treatment improved the efficiency of retinal organoid production to 100% based upon SIX6-GFP expression. (*I*–*M*) Inhibition of BMP4 signaling with LDN-193189, using both the traditional and standardized differentiation methods, produced organoids that lacked expression SIX6-GFP, indicating an inability to differentiate toward a retinal lineage. (*N* and *O*) Quantification of the size and circularity of traditional vs. standardized methods of retinal organoid differentiation at Day 25. Error bars represent SEM (*P < 0.05, ***P < 0.001, and ****P < 0.0001). (Scale bars equal 500 µm (*A*–*L*) and n = 3 biological replicates (*M*–*O*).)

25 when compared to organoids differentiated using the traditional methods of differentiation (Fig. 3 *N* and *O*). Interestingly, aggregates differentiated using the standardized method without BMP4 were also variable in their individual organoid size and shape (Fig. 3 *E* and *F*), suggesting that perhaps some variability observed in traditional methods may be due to the presence of nonretinal populations influencing developing retinal organoids.

Next, we sought to confirm that this improved retinal organoid differentiation efficiency to 100% purity could be replicated across multiple other cell lines. Thus, we tested a total of six stem cell lines (*SI Appendix*, Table S1) and differentiated each cell line into retinal organoids until a total of 25 d of differentiation, using both the traditional and standardized methods. These cell lines were chosen to represent a variety of cell line characteristics, including both human embryonic stem cells and human induced pluripotent stem cells, as well as cell lines from both male and female sources. While many of these cell lines have been previously shown to effectively give rise to retinal organoids, we also included a line that we have observed to be typically inefficient at retinal organoid specification (WTC11). Finally, to ensure that our results were not solely due to the use of popular stem cell lines that have been widely used due to desirable differentiation characteristics, we also generated a newly reprogrammed iPS cell line (JM2019) and tested this cell line for its capacity for retinal differentiation. Retinal organoids were differentiated via either traditional methods or with standardized methods at an original seeding density of 2,000 cells per well and stimulated to differentiate to a retinal lineage in the presence of BMP4, as described above. As these other cell lines lacked the SIX6:GFP reporter, retinal organoids derived from these cell lines were then fixed, cryosectioned, and stained for the retinal progenitor marker VSX2 (formerly CHX10) to determine retinal organoid differentiation efficiency. Following the traditional method of retinal organoid differentiation, highly variable yields of retinal organoids were observed, ranging from as little as approximately 30% (WTC11) to greater than 80% efficiency (H7 and H9), depending on the cell line used (Fig. 4 *A*–*F* and *M*–*R*). Conversely, the differentiation of retinal organoids following standardized methods consistently produced 100% efficiency based upon VSX2 immunoreactivity across all hPSC lines (Fig. 4 *G*–*L* and *M*–*R*), demonstrating that the differentiation of retinal organoids through these standardized methods enables the ability to derive retinal organoids at 100% efficiency across multiple hPSC lines.

Leveraging Efficient Retinal Organoid Formation As a Tool for the Study of Human Retinogenesis. Previous studies have leveraged retinal organoids as a model system to examine early stages of human retinogenesis (5, 11, 12, 14, 23), yet these studies were dependent upon the definitive identification of retinal organoids after at least a month of differentiation. Given the ability to now specify the differentiation of retinal organoids at 100% efficiency through the use of standardized approaches including early treatment with BMP4, as well as the ability to

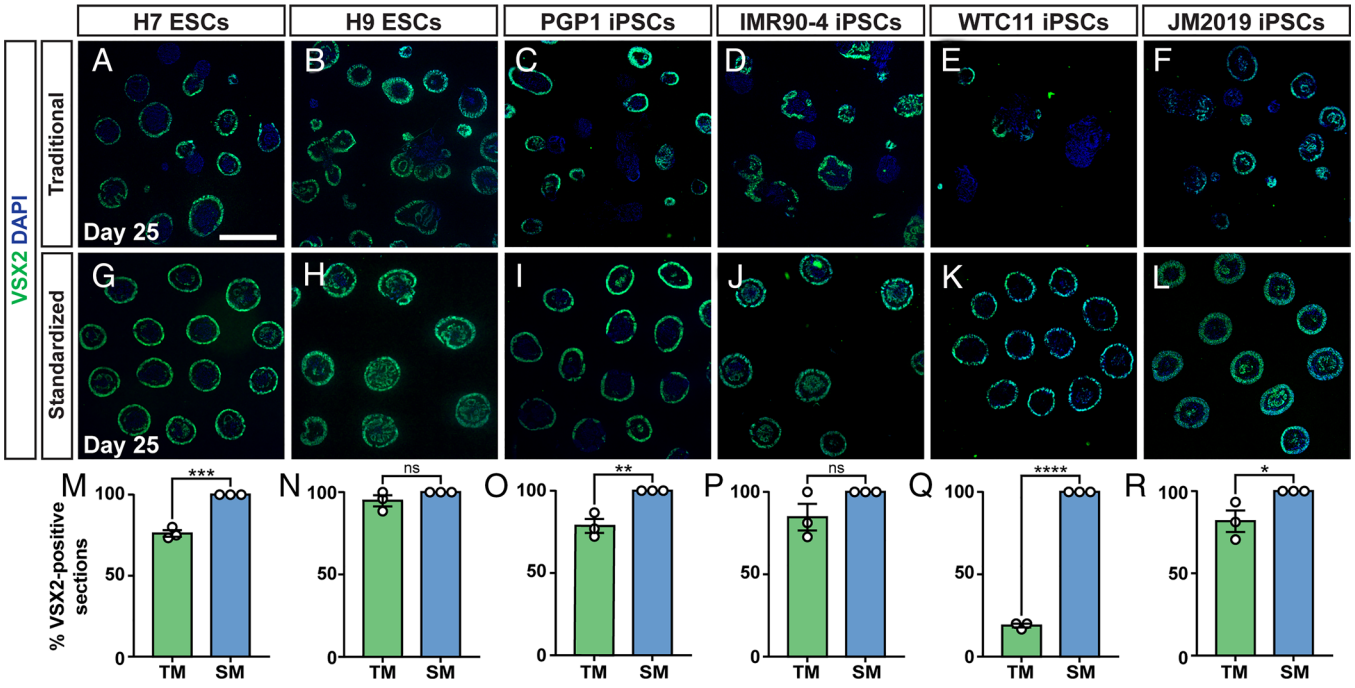

Fig. 4. Reproducibility of highly efficient retinal organoid differentiation with standardized methods across hPSC lines. (*A–F*) Organoids differentiated using the traditional method across multiple hPSC lines until Day 25. (*G–L*) Organoids differentiated using the standardized method across the same hPSC lines until Day 25. (*A–L*) VSX2 is stained in green and DAPI is stained in blue. (*M–R*) Quantification of retinal organoid differentiation efficiency demonstrating that the traditional method of differentiation generated variable yields of VSX2-positive retinal organoids depending on the cell line used, while organoids differentiated using the standardized method produced 100% VSX2-positive organoids consistently across all hPSC lines. Error bars represent SEM. (**P* < 0.05, ***P* < 0.01, ****P* < 0.001, and *****P* < 0.0001). The scale bar equals 1,000 μm (*A–L*) and n = 3 biological replicates (*M–R*).

completely block retinal fate determination by inhibiting BMP signaling resulting in cortical forebrain differentiation, we chose to pursue the analysis of the earliest transcriptional events in human retinal fate determination. Previous studies have demonstrated that differentiating cells at Day 6 represents the most primitive stage of neuroepithelial specification (12, 31, 32), with the ability to give rise to retinal as well as other CNS lineages and thus, prior studies have leveraged this timepoint for treatment with BMP4 to induce greater retinal specification (23, 30). Thus, we decided to assess transcriptional features of retinal fate specification through RNA-seq analyses (33), comparing primitive neuroepithelial (Day 6) with early retinal (Day 8 BMP4) and early cortical forebrain (Day 8 LDN-193189). Total RNA was collected from cellular aggregates on Day 6 before any treatment, and then also collected on Day 8 after treatment with either BMP4 or LDN-193189 at Day 6 (Fig. 5*A*). As the ability to completely modulate retina vs. cortical forebrain fate specification at 100% efficiency is essential for these experiments, we also maintained some of these cultures until Day 25 of differentiation, at which point we then confirmed that presumptive retinal organoids expressed SIX6:GFP at 100% efficiency before performing mRNA-seq analyses of Day 6 and Day 8 samples, while LDN-treated cortical forebrain organoids completely lacked GFP expression.

We initially analyzed Day 8 BMP4-treated (early retinal) compared to Day 6 (primitive neuroepithelial) cultures to identify the earliest transcriptional changes associated with the acquisition of a retinal fate from a more primitive neuroepithelial population (Fig. 5 *B* and *C*). Intriguingly, after only 2 d of BMP4 treatment, we observed a significant upregulation in the expression of known retinal developmental genes including SIX6, RAX, LHX9, VSX2, and PAX6 (34, 35), as well as pathway analyses indicating an overall decrease in neuronal-associated differentiation signatures more associated with the forebrain at this developmental timepoint, in favor of signatures associated with BMP responsiveness as well as changes to the matrisome (Fig. 5 *B* and *C*). Interestingly, while expression of transcripts such as SIX6 was differentially expressed at Day 8, the expression of the corresponding protein was delayed until nearly Day 10, based upon timelapse imaging of the SIX6:GFP reporter (Movie S2). Additionally, some other differentially expressed genes (DEGs) were identified at this early stage that were less expected, including genes with known roles in the retina such as MAB21L2 and DIO3. Next, we sought to determine transcriptional changes associated with the acquisition of a cortical forebrain phenotype (Day 8 LDN-193189) compared to the more primitive neuroepithelial cultures (Day 6). In this context, we were able to identify the upregulation of numerous forebrain-associated transcripts, including FOXG1, NEUROD1, and MAP2 (36), as well as increased activation of biological pathways associated with neuronal maturation (Fig. 5 *D* and *E*). Finally, when comparing Day 8 BMP4-treated (early retinal) with Day 8 LDN-treated (early cortical forebrain), we observed an increase in many retinal-specific genes including VSX2, SIX6, and RAX, and a decrease in more cortical/forebrain-related genes including FOXG1 and MAP2 (Fig. 5 *F* and *G*). Interestingly, numerous matrisome-associated genes were also up-regulated in the early retinal population, perhaps suggestive of activation of key components associated with the high degree of cellular organization found within retinal organoids. Taken together, the ability to selectively differentiate retinal vs. cortical forebrain organoids at 100% efficiency from a common neuroepithelial progenitor allowed for the insight into some of the earliest transcriptional changes associated with retinal fate specification, long before any human donor tissue would normally be available for such investigations.

Expedited Retinal Ganglion Cell and Photoreceptor Differentiation. To explore how this increased reproducibility of retinal organoids may contribute to their subsequent differentiation into

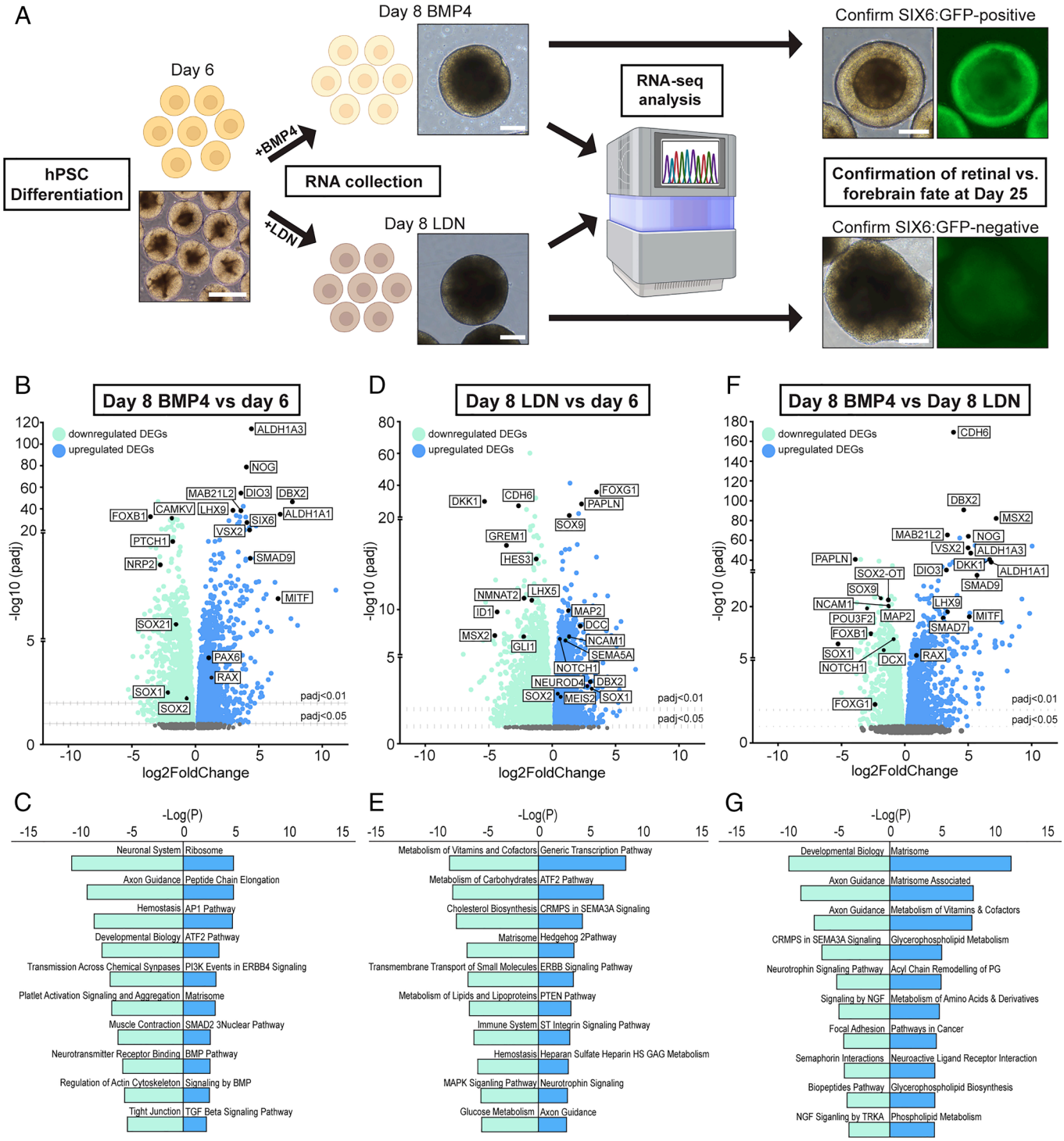

Fig. 5. Standardized methods of retinal organoid differentiation allow for the analysis of transcriptional changes associated with the earliest stages of retinogenesis. (*A*) Schematic of organoid sample collection and RNA-seq analyses of early-stage cellular aggregates. (*B*–*G*) Volcano plots showing differentially expressed genes (DEGs) and associated pathway enrichment analyses that were significantly up-regulated (blue) or down-regulated between (aquamarine). (*B* and *C*) Day 8 after treatment with BMP4 and Day 6 untreated, (*D* and *E*) Day 8 after treatment with LDN193-189 and Day 6 untreated, and (*F* and *G*) Day 8 after treatment with BMP4 and Day 8 after treatment with LDN-193189. DEGs, **P*adj < 0.05, ***P*adj < 0.01. (Scale bars, 500 μm in (*A*) for Day 6 and 100 μm in (*A*) for Day 8 and Day 25.)

some of the major retinal cell types in a stratified manner, we further differentiated organoids for a total of up to 150 d, at which point major cell types including retinal ganglion cells (RGCs) and photoreceptors are specified (Fig. 6). Initially, we differentiated retinal organoids for a total of 30 d, at which point previous studies have demonstrated that RGCs have begun to be specified (3, 15, 23). At this stage, retinal organoids derived through standardized methods exhibited a greater degree of consistency in their size and shape compared to those derived from traditional methods (Fig. 6 *A* and *B*). To assess the differentiation state of RGCs as the first retinal cell type specified, we utilized a newly developed human induced pluripotent stem cell reporter line in which an EGFP reporter was edited into the 3′ end of the BRN3b locus, similar to prior studies that have used a tdTomato reporter in

human embryonic stem cells (37). Interestingly, while 30 d of differentiation is near the beginning of RGC differentiation in previous studies (3, 15, 23) as well as the current study using traditional methods, we found a much greater degree of RGC differentiation in retinal organoids derived using the standardized method (Fig. 6 *C*–*F*), suggesting that these standardized methods may also expedite the differentiation of retinal cell types. Indeed, qRT-PCR performed on organoid samples from both methods from 30 to 80 d of differentiation demonstrated an increased expression of BRN3b as an indicator of RGCs at earlier stages of differentiation when differentiated using standardized methods, while BRN3b expression in the traditional method catches up with the standardized method by Day 80 (Fig. 6*G*). Next, we sought to determine whether there was an additional pool of cells in the traditional method that did not exist in the standardized method and could account for the increase in BRN3b expression, such as a residual pool of VSX2-positive retinal progenitors. Interestingly, using qRT-PCR analyses, we did not observe a difference in VSX2 mRNA expression at Day 40 between the traditional and standardized methods, although BRN3b expression was significantly increased (*SI Appendix*, Fig. S4*A*). However, we found that the expression of SOX1 was significantly higher in the traditional method compared to standardized methods (*SI Appendix*, Fig. S4*A*), suggesting that the traditional method likely contains a small but present population of forebrain cell types that contaminate retinal populations, and further emphasizes the purity of retinal progenitors found in organoid populations derived through standardized methods.

Next, we examined whether this expedited differentiation at Day 30 was carried forward into the differentiation of photoreceptors as a later generated retinal cell type. After a total of 60 d of differentiation, a timepoint at which previous studies have demonstrated the onset of CRX expression as a marker of early photoreceptor progenitor cells (23, 25, 26), we observed that while retinal organoids became somewhat more irregular in shape, they still appeared more consistent than those derived through traditional methods (Fig. 6 *H* and *I*). Additionally, while traditional methods typically resulted in a thin layer of CRX-positive photoreceptor progenitor cells along the apical edge of organoids, organoids derived from standardized methods had more robust expression of CRX along the apical edges, often consisting of multiple layers of CRX-positive cells (Fig. 6 *J*–*M*). Additionally, qRT-PCR analysis helped to

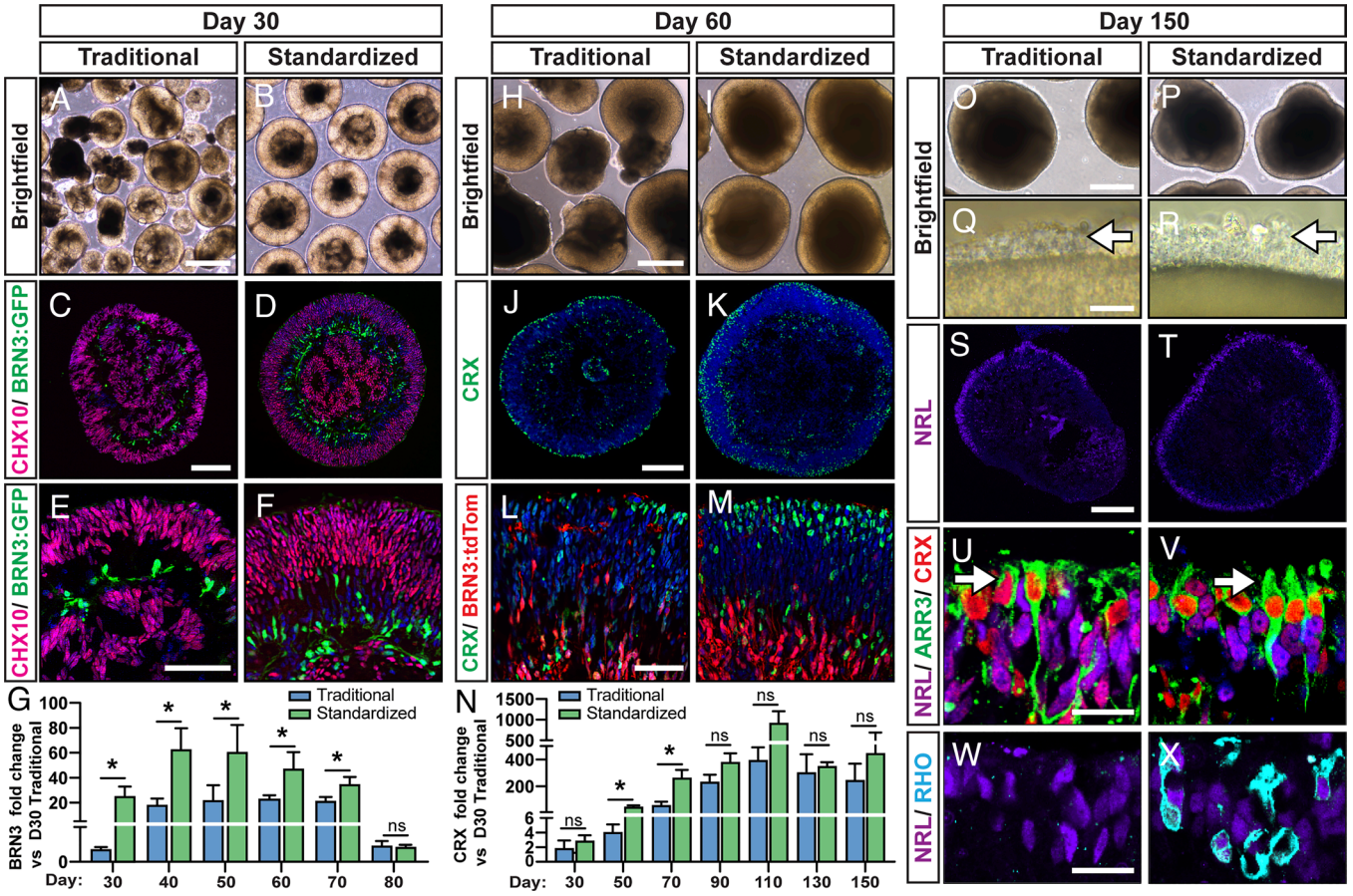

Fig. 6. Expedited retinal ganglion cell and photoreceptor differentiation. Retinal organoids at 30 d, 60 d, and 150 d of total differentiation, derived using both the traditional and standardized methods. (*A* and *B*) Brightfield images of retinal organoids at Day 30 of differentiation that were derived using a BRN3b:GFP reporter cell line, (*C*–*F*) whole sections and high magnification images of retinal organoids expressing the retinal progenitor marker VSX2 (magenta) and the retinal ganglion cell (RGC) marker BRN3b (green), identified with a BRN3b:GFP reporter. (*G*) qRT-PCR analyses of retinal organoids differentiated using both the traditional and standardized methods from Day 30 until Day 80 showing mRNA expression of BRN3b normalized to the Day 30 traditional method as the control. (*H* and *I*) Brightfield images of retinal organoids taken after 60 d of differentiation, (*J*–*M*) whole sections and high magnification images of retinal organoids expressing the cone and rod photoreceptor marker CRX (green) and the retinal ganglion cell (RGC) marker BRN3b:tdTomato (red). (*N*) qRT-PCR analyses of retinal organoids differentiated using both the traditional and standardized methods from Day 30 until Day 150 showing mRNA expression of CRX normalized to the Day 30 traditional method as the control. (*O*–*R*) Low-magnification and high-magnification brightfield images of retinal organoids at Day 150 showing photoreceptor outer segments. (*S*–*X*) Whole sections and high magnification images of retinal organoids at 150 d showing the expression of the cone and rod photoreceptor marker CRX (red), the rod photoreceptor markers NRL (purple) and Rhodopsin (blue), as well as the cone photoreceptor marker ARR3 (green). DAPI (blue) for all images. Error bars represent SEM. (Scale bars equal 500 μm (*A*, *B*, *H*, *I*, *O*, and *P*) or 100 μm (*C* and *D*) or 200 μm (*J*, *K*, *S*, and *T*) or 50 μm (*E*, *F*, *L*, *M*, *Q*, and *R*) and 20 μm (*U*–*X*). n = 3 to 6 biological replicates (*G* and *N*).

demonstrate that CRX expression was indeed initiated earlier in standardized method organoids, with the onset occurring before 50 d of differentiation compared to 60 d in the traditional method (Fig. 6*N*). We similarly confirmed this expedited photoreceptor differentiation through analyses of OTX2 expression, in which qRT-PCR analyses demonstrated a significant increase in OTX2 mRNA expression when organoids were differentiated using the standardized method at early stages compared to the traditional method (*SI Appendix*, Fig. S4*B*). However, at Day 90 no significant differences were observed in the expression of either OTX2 or CRX, suggesting that the traditional method of differentiation caught up with the standardized method (Fig. 6*N* and *SI Appendix*, Fig. S4*B*), further highlighting the expedited nature of development within standardized method retinal organoids. Additionally, at later stages of differentiation using the standardized method, some but not all retinal organoids also formed clumps of retinal pigment epithelium (RPE), similar to the traditional method of differentiation (*SI Appendix*, Fig. S5).

Subsequently, we assessed the effects of standardized methods of differentiation upon later stages of photoreceptor differentiation, examining retinal organoids after a total of 150 d of differentiation, a timepoint at which previous studies have associated with the onset of rod photoreceptor differentiation. Initially, the most obvious difference at this stage was found in the appearance of photoreceptor segments extending out of the apical edge of retinal organoids, with these extensions more prominent in organoids derived from standardized methods (Fig. 6 *O*–*R*). Additionally, 100% of all retinal organoids differentiated until Day 150 using the standardized method exhibited photoreceptor outer segments with a full brush border (meaning inner/outer segments were observed around the entire organoid), whereas 6.00% ± 3.79% of retinal organoids differentiated using the traditional method exhibited a full brush border of photoreceptor outer segments and 26.33% ± 15.30% (SEM) of traditional retinal organoids exhibited a partial brush border of photoreceptors (*SI Appendix*, Fig. S6). We also observed a greater degree of NRL expression along the outer edges of organoids following standardized methods (Fig. 6 *S* and *T*), as well as more prominent expression of cone arrestin (ARR3), particularly in those segments extending outward from the organoid (Fig. 6 *U* and *V*). Finally, while NRL expression was observed at this timepoint following both traditional and standardized methods, the expression of rhodopsin was almost exclusively observed within standardized method organoids (Fig. 6 *W* and *X*), compared to later stages in retinal organoids derived using traditional methods, further supporting the expedited differentiation of cell types in the standardized approach.

Discussion

The results of the current study demonstrate robust improvements to existing retinal organoid differentiation protocols (5, 15, 23, 38) that greatly streamline the differentiation process, resulting in highly reproducible retinal organoids relative to their size and shape, and perhaps most importantly, at an efficiency of 100% purity across multiple cell lines. The ability to yield pure populations of retinal organoids with high consistency in their composition across multiple cell lines greatly reduces previous issues with efficiency between cell lines that were difficult to direct to a retinal lineage (27). Additionally, given the high degree of variability between individual retinal organoids following previous protocols (5, 15, 23), experimental comparisons often needed to be made between populations of organoids to account for this variability. However, with the more standardized methods outlined in the current study, it may now be possible in some applications to make comparisons more directly between individual organoids, as the variability between organoids with these technical improvements has been proven to be considerably reduced.

Throughout these studies, it became apparent that the size of initial cellular aggregates at the onset of differentiation was critical for their ability to effectively yield retinal lineages and organoids. Traditional differentiation methods introduce tremendous variability in the size of initial aggregates due to the use of enzymes such as dispase or collagenase that lift entire colonies of undifferentiated stem cells from the plate to generate each aggregate (38, 39). Given the variability in the size of stem cell colonies, this variability was then carried forward into the differentiation process, hindering the ability to enhance retinal differentiation consistency within the cellular population. Through the use of quick reaggregation methods described in this study, we were able to tightly regulate the size of cellular aggregates at the onset of differentiation, thereby removing a considerable source of variability in subsequent retinal differentiation. Demonstrating the importance of the size of initial cellular aggregates, we observed that when cellular aggregates were constructed with too few cells (e.g., 500 cells per well or less), we lost the ability to achieve the 100% purity of retinal organoid differentiation. By extension, it will be of interest in future studies to adopt these types of approaches to the study of microphthalmia/anophthalmia, particularly to better elucidate whether gene variants resulting in these disorders prevent retinal specification or simply reduce the size of the retinal progenitor pool and then consequently, this reduced retinal progenitor pool is insufficient to allow formation of 3D retinal tissue.

While we have found that the use of quick reaggregation methods using single-cell suspensions was critical to achieving the 100% purity of retinal organoids with more highly consistent size and shape, this is not the first study to use this type of quick reaggregation method to yield retinal organoids. Indeed, several other studies to date have attempted to use these types of approaches as well, yet they have not achieved the purity of retinal organoid differentiation observed in this study (14, 25, 40). Several factors may contribute to these differences, including variations in the underlying differentiation protocol used in which some protocols may be more robust to yield retinal organoids than others. It is also possible that some of the reagents used may vary in quality depending upon the commercial source, and we have noticed a decreased efficiency of retinal differentiation, for example, depending on the source of recombinant BMP4 protein. Additionally, prior studies have often kept these cellular aggregates in the 96-well plates in some cases for several days (2, 41, 42), whereas our approaches have aggregated the cells for 1 d in the undifferentiated state in mTeSR1 maintenance medium before starting to transition into neural induction medium (NIM) for one more day before removing aggregates from the 96-well plate and transferring the population to a new culture dish. In this context, some of our preliminary studies kept aggregates in 96-well plates beyond the first day of differentiation, in which case we observed increasing variability among aggregates, suggesting that when aggregates were allowed exposure to paracrine signals early in a combined culture, these signals may aid in the synchronized differentiation of each developing organoid.

We also explored the dependency of retinal organoid differentiation upon signaling from BMP4, which has been used to aid in retinal differentiation from hPSCs (23). This approach was initially incorporated into the differentiation process by Kuwahara et al. (30) and subsequently adopted by numerous other groups, including our own (8, 16, 43–45). However, while it has been demonstrated that BMP4 supplementation can enhance the

differentiation of retinal organoids, it has not yet been shown that the retinal differentiation process itself is dependent upon BMP signaling. In the current study, we demonstrated that BMP4 supplementation enhanced retinal differentiation in both traditional and standardized methods, while the inhibition of BMP signaling by the small molecule LDN-193189 completely inhibited retinal organoid differentiation. These results demonstrate that the derivation of retinal organoids is dependent upon BMP signaling and that previous traditional methods of retinal organoid differentiation that lacked exogenous BMP4 signaling must have leveraged the endogenous production of BMPs by the differentiating cellular aggregates.

Prior studies exploring the differentiation of retinal organoids often also observed the differentiation of other nonretinal, forebrain-like organoids in parallel with the derivation of retinal organoids (5, 38). These two parallel lineages have not necessarily been unexpected, as both the retina and the forebrain are derived from the early telencephalic region of the developing neural tube (35). As such, these lineages are closely related and likely segregate through only minor differences in their developmental trajectories. Through the use of newly standardized methods, we observed that the differentiation of cells to either retina or forebrain lineages could be tightly regulated in an "On/Off" fashion through the activation or inhibition of BMP signaling with the addition of either BMP4 or LDN-193189, respectively. Thus, we believed this to be an opportunity to explore the use of organoid models as a platform to study the earliest stages of human retinal fate specification, far earlier than would be possible with human donor tissue. Additionally, while some other studies have also attempted to explore differences between early retinal and forebrain lineages in this manner (5), those studies were entirely dependent upon the prior specification and phenotypic identification of these two populations, which is only possible more than 2 wk after this cell fate determination has occurred.

Thus, with our newfound ability to completely regulate the retina vs. forebrain cell fate determination event with standardized methods using either BMP4 or LDN-193189, we decided to explore the earliest transcriptional changes that underlie these differentiation events through the use of RNA-seq approaches, exploring samples collected at either Day 6 or Day 8 of differentiation. Samples collected at Day 6 represented a common progenitor with competency to yield either retina or forebrain (and likely other lineages given appropriate induction cues) prior to the addition of either BMP4 or LDN-193189. At Day 8 of differentiation, we collected samples that had been treated with either BMP4 or LDN-193189, representing some of the earliest changes that could be observed associated with the retina vs. forebrain fate determination, long before identifying features of each lineage were manifested in differentiating cultures. Within these experiments, it was noteworthy and somewhat surprising to observe the onset of gene expression clearly related to either retinal or forebrain lineages at such an early timepoint. Indeed, some expected genes were observed to properly segregate, such as the increased expression of VSX2, RAX, and MITF in Day 8 BMP4-treated cultures compared to both Day 6 as well as Day 8 LDN-193189-treated cultures. However, these approaches also uncovered the differential expression of other genes that may play influential roles in the formation of retinal organoids, such as the increased expression of CDH6 that may contribute to the self-organization of cells within retinal organoids (46), as well as the expression of genes such as DIO3 which may indicate a role for thyroid hormone signaling early in the separation of retina and forebrain lineages. The early expression of genes such as MAB21l2 [associated with microphthalmia (47)] and ABCA4 [mutated in Stargardt's disease (48)] also suggests that perhaps some disease-associated changes may also be identified at these earliest differentiation stages. Interestingly, core matrisome-related genes that have previously been shown to be abundant in retinal ECM including collagen alpha-1 (COL12A1), the glycoprotein LAMA5, and the matrisome-associated annexins/plexins (ANXA2, PLXNB2, and PLXNA1) (49) were also up-regulated in the Day 8 BMP4-treated cultures, suggesting that these core matrisome genes, as well as matrisome-associated genes, may also be important for retinal vs. forebrain specification and may contribute to the maturation and organization of retinal cells within retinal organoids.

Upon the differentiation of early retinal organoids, we also observed the expression of markers associated with fully differentiated retinal cell types at stages earlier than those predicted by previous studies (15, 23). The use of cell type-specific fluorescence reporters such as the BRN3b:tdTomato:Thy1.2 or BRN3b:EGFP:Thy1.2 reporters for RGCs allowed us to identify the differentiation of RGCs as early as 20 d of differentiation using standardized methods compared to nearly 30 d of differentiation with traditional methods. This expedited differentiation was also associated with a maintained higher degree of consistency in the size and shape of retinal organoids, with the organization of cell types appearing to be more consistent as well. The expedited differentiation of cell types was not limited to RGCs, as we also observed an earlier start to the differentiation of photoreceptors based upon the onset of expression of CRX, longer and more defined photoreceptor outer segments extending from the surface of retinal organoids, as well as the earlier expression of rhodopsin. While it is unclear exactly why cell types appeared to differentiate more quickly following newly standardized methods compared to the traditional methods, it is likely to be due at least in part to the greater synchronization of cells and their differentiation that is afforded by the more consistent size and shape from the outset of differentiation.

Prior studies have also suggested a staging system based upon the differentiation of various cell types within retinal organoids (23). These stages were not only based upon the presence of certain differentiated cell types and/or the expression of cell type-specific markers but also how long the organoids had differentiated. Given the expedited differentiation of cell types observed in the current study, these timepoints associated with retinal organoid stages do not neatly line up anymore. Indeed, it was previously suggested that "Stage 1" retinal organoids defined by the onset of RGCs and some rare starburst amacrine cells begins at Day 30 of differentiation, whereas "Stage 2" retinal organoids began after 70 d of differentiation and are characterized by the presence of photoreceptor precursors in addition to RGCs. Within the current study, however, we began to observe RGC specification closer to 20 d of differentiation, earlier that the suggested start of "Stage 1" at Day 30. Similarly, we observed the presence of photoreceptor precursors, based upon the expression of CRX, as early as Day 40 of differentiation, far earlier than the previously described Day 70 timepoint. Taken together, the results of the current study may necessitate a revisiting of these retinal organoid staging approaches, as initially recommended (23).

With the ability to yield retinal organoids at 100% efficiency with greatly enhanced reproducibility, it is still important to note that several parameters must be met in order to achieve this consistency. Not unlike any other study with hPSCs, it is essential for the starting population of stem cells to be highly pure without any signs of spontaneous differentiation, as some trace amounts of spontaneous differentiation at the outset of differentiation can provide adverse signaling factors to inhibit retinal specification. Our results also demonstrate that the size of starting cellular

aggregates is critical for the 100% efficient yield of retinal organoids, and we have recommended a starting cell density of 2,000 cells per well that both ensures efficient specification of retinal organoids, while also being conservative in the overall number of cells needed for experimentation. Additionally, unlike prior studies that often maintain cell aggregates in individual wells for multiple days (41, 42), we found that the early removal of these aggregates after just 1 d of differentiation helped to maintain reproducibility while also retaining the highly efficient derivation of retinal organoids. The results of these studies will be highly important for future applications of retinal organoids, in which the reduction of variability will likely facilitate not only the efficient derivation of retinal organoids across an array of cell lines, as well as enable more direct experimental comparisons to be made not only across larger populations of organoids, but also small numbers of organoids and even perhaps between individual organoids.

Materials and Methods

Maintenance of hPSC Cultures. hPSC lines used in this study included the embryonic stem cell lines H7 and H9, as well as iPSC lines IMR90-4, WTC11, PGP1, and JM2019 (*SI Appendix*, Table S1). These cell lines also represented both male (WTC11, PGP1, and IMR90-4) and female (H7, H9, and JM2019) sources. Among these, some cell lines were edited for some studies to express fluorescent reporters, including the H7 cell line (BRN3b-tdTomato-Thy1.2), IMR90-4 (SIX6-GFP), and JM2019 (BRN3b-EGFP-Thy1.2). All hPSC lines were maintained on six well-plates coated with either Matrigel or Geltrex and grown in mTeSR1 or mTeSR PLUS medium. Media were changed daily to maintain the pluripotency of hPSCs. At approximately 60 to 70% confluency, hPSCs were passaged using either Accutase or ReLeSR, and either expanded in similar conditions or used for differentiation experiments.

iPSC Reprogramming. To establish the JM2019 iPSC line, human peripheral blood mononuclear cells (PBMCs) were obtained from StemCell Technologies (catalog 70025.1), and iPSCs were generated by reprogramming of PBMCs using the CytoTune-iPS 2.0 Sendai Reprogramming Kit (Life Technologies catalog A16517) following the manufacturer's instructions. Details of reprogramming process can also be found within *SI Appendix*.

CRISPR/Cas9 Gene Editing. Gene-edited cell lines used in this study included the H7 BRN3b-tdTomato-Thy1.2 reporter line, the IMR90-4 SIX6-GFP reporter line, and the JM2019 BRN3b-EGFP-Thy1.2 reporter line. The establishment of the first two lines was previously described (28, 37). For the editing of the JM2019 iPSC line to possess the BRN3b-EGFP-Thy1.2 reporter, we followed strategies previously described by Sluch et al. (37), with the exception that the tdTomato gene was replaced with an EGFP sequence. Details regarding the process of CRISPR/Cas9 gene editing of this cell line can be found within *SI Appendix*.

Retinal Organoid Differentiation from hPSCs. hPSCs were differentiated into retinal organoids using previously established protocols as a control "traditional" method of differentiation (5, 50, 51). For the establishment of the experimental "standardized" method of differentiation, hPSCs colonies at approximately 70% confluency were dissociated into single cells using Accutase and seeded at different densities ranging from 250 to 8,000 cells per well. On Day 1 of differentiation, cellular aggregates were transferred to standard polystyrene 10 cm dishes, and all spent media were replaced with 6 mL of fresh mTeSR1/mTeSR PLUS, as well as 6 mL of fresh Neural Induction Medium (NIM). On Day 2, 6 mL of media was removed and 6 mL of fresh NIM was added to each dish, while on Day 3, aggregates were transferred to 12 mL of fresh complete NIM medium. On Day 6, 12 mL of fresh NIM with either 50 ng/mL of BMP4 or 200 nM of LDN-193189 was added to the cellular aggregates to either activate or inhibit BMP signaling, respectively. On Day 8 of differentiation, 500 µL of Fetal Bovine Serum (FBS) was then added directly to each well of a six-well plate to ensure cellular aggregates adhere to wells. On Day 16, organoids were manually removed from the plates and transferred to 10 cm dishes containing Retinal Differentiation Medium [RDM, consisting of DMEM/F12 (3:1), 2% B27 supplement, 1% MEM nonessential amino acids, and 1× anti-anti] with 1% fetal bovine serum (FBS). Further details of retinal organoid differentiation, including reconstitution of all supplements, are described in *SI Appendix*, *Methods*.

Immunocytochemistry and Microscopy Analyses. For brightfield imaging of retinal organoids, samples were imaged at indicated timepoints using a Nikon Eclipse TS2R-FL microscope, with images captured with a Nikon DS-Ri2 color digital camera. For histological analyses, retinal organoids were processed for immunocytochemistry and microscopy following previously described procedures (52). Detailed methods can be found in *SI Appendix*, and a list of antibodies used can be found in *SI Appendix*, Table S2.

RNA-Seq Analyses. To assess the transcriptional profile of cells at the earliest stages of retinal fate specification, hPSC aggregates were differentiated as described above for the first 6 d of the protocol and then split into three conditions: Day 6 baseline, Day 8 BMP4 (treated from Days 6 to 8), and Day 8 LDN treated (treated from Days 6 to 8). Total RNA was collected from untreated aggregates on Day 6 and treated aggregates on Day 8 using the Picopure RNA extraction kit (Life Technologies). mRNA-seq was then performed as previously described (53, 54). The GEO accession number for the bulk RNA-seq dataset is GSE254830. Additional detailed methods can also be found in *SI Appendix*.

qRT-PCR Analyses. For qRT-PCR analyses, ~10 retinal organoids per batch were collected at Days 30, 40, 50, 60, and 70, and total RNA was extracted using the Picopure RNA extraction kit (Life Technologies) following the manufacturer's instructions. cDNA was then synthesized using the High Capacity RNA-to-cDNA Kit (Applied Biosystems), and qRT-PCR analyses were performed using a Quant Studio 7 Flex system (Applied Biosystems) with SYBR green (Life Technologies), using primers as specified in *SI Appendix*, Table S3. Gene expression was defined using a comparative Ct method, normalized to β-actin. The ΔCt value was normalized to the average ΔCt value of the traditional method Day 30 organoids to calculate ΔΔCt, and fold change was calculated using the formula ($2^{-\Delta\Delta Ct}$), as previously described (55).

Quantification and Statistical Analysis. For imaging, cellular aggregates and organoids were swirled into the middle of the dish, and images were taken within the center of the aggregate and/or organoid population for representative purposes. All calculations were measured blinded to minimize bias. The size and circularity of hPSC-derived aggregates and/or organoids were quantified using ImageJ by calculating the area (mm^2) and circumference, with details of these calculations found in Supplemental Information. To quantify the percentage of organoids that adopted a retinal fate based upon staining for VSX2, this was calculated by dividing the total number of VSX2 (green)-positive sections by the total number of DAPI sections (blue). Serial sectioning was performed for all organoids and cell lines. A Student's *t* test or a one-way ANOVA followed by Tukey's post hoc analysis was used for statistical analyses, as indicated.

Data, Materials, and Software Availability. All study data are included in the article and/or supporting information. RNA-seq data has been deposited to GEO under accession number GEO: GSE254830 (33).

ACKNOWLEDGMENTS. We thank Dr. Karl Wahlin for sharing the SIX6:GFP iPS cell line and Dr. Don Zack for sharing the BRN3b:tdTomato:Thy1.2 cell line. We also thank the Indiana University Center for Medical Genomics for assistance with RNA-seq analyses. Grant support was provided by the National Eye Institute (R01EY033022 and U24EY033269 to J.S.M.), the BrightFocus Foundation (G2020369 to J.S.M.), and the Gilbert Family Foundation (923016 to J.S.M.). Support for this project was also provided by the Sarah Roush Memorial Fellowship from the Indiana Alzheimer's Disease Center (C.G.), the BrightFocus Postdoctoral Fellowship (G2022003F to C.G.), a Shaffer Grant from the Glaucoma Research Foundation (C.G.), as well as a Cagiantas scholarship from the Indiana University School of Medicine (J.H.).

Author affiliations: [a]Department of Pharmacology and Toxicology, Indiana University School of Medicine, Indianapolis, IN 46202; [b]Stark Neurosciences Research Institute, Indiana University School of Medicine, Indianapolis, IN 46202; [c]Department of Biology, Indiana University Purdue University Indianapolis, Indianapolis, IN 46202; [d]Department of Medical and Molecular Genetics, Indiana University School of Medicine, Indianapolis, IN 46202; [e]Department of Medicine, Indiana University School of Medicine, Indianapolis, IN 46202; [f]Department of Biology, University of Kentucky, Lexington, KY 40506; and [g]Department of Ophthalmology, Indiana University School of Medicine, Indianapolis, IN 46202

1. A. Gonzalez-Cordero *et al.*, Recapitulation of human retinal development from human pluripotent stem cells generates transplantable populations of cone photoreceptors. *Stem Cell Rep.* **9**, 820–837 (2017).
2. D. Hallam *et al.*, Human-induced pluripotent stem cells generate light responsive retinal organoids with variable and nutrient-dependent efficiency. *Stem Cells* **36**, 1535–1551 (2018).
3. C. M. Fligor *et al.*, Three-dimensional retinal organoids facilitate the investigation of retinal ganglion cell development, organization and neurite outgrowth from human pluripotent stem cells. *Sci. Rep.* **8**, 14520 (2018).
4. T. Nakano *et al.*, Self-formation of optic cups and storable stratified neural retina from human ESCs. *Cell Stem Cell* **10**, 771–785 (2012).
5. J. S. Meyer *et al.*, Optic vesicle-like structures derived from human pluripotent stem cells facilitate a customized approach to retinal disease treatment. *Stem Cells* **29**, 1206–1218 (2011).
6. K. C. Huang *et al.*, Morphological and molecular defects in human three-dimensional retinal organoid model of X-linked juvenile retinoschisis. *Stem Cell Rep.* **13**, 906–923 (2019).
7. A. Lane *et al.*, Modeling and rescue of RP2 retinitis pigmentosa using iPSC-derived retinal organoids. *Stem Cell Rep.* **15**, 67–79 (2020).
8. S. J. Mayerl *et al.*, Human retinal organoids harboring IMPG2 mutations exhibit a photoreceptor outer segment phenotype that models advanced retinitis pigmentosa. *Stem Cell Rep.* **17**, 2409–2420 (2022).
9. N. K. Mullin *et al.*, Multimodal single-cell analysis of nonrandom heteroplasmy distribution in human retinal mitochondrial disease. *JCI Insight* **8**, e165937 (2023).
10. K. B. VanderWall *et al.*, Retinal ganglion cells with a glaucoma OPTN(E50K) mutation exhibit neurodegenerative phenotypes when derived from three-dimensional retinal organoids. *Stem Cell Rep.* **15**, 52–66 (2020).
11. M. J. Phillips *et al.*, Modeling human retinal development with patient-specific induced pluripotent stem cells reveals multiple roles for visual system homeobox 2. *Stem Cells* **32**, 1480–1492 (2014).
12. J. S. Meyer *et al.*, Modeling early retinal development with human embryonic and induced pluripotent stem cells. *Proc. Natl. Acad. Sci. U.S.A.* **106**, 16698–16703 (2009).
13. P. Wahle *et al.*, Multimodal spatiotemporal phenotyping of human retinal organoid development. *Nat. Biotechnol.* **41**, 1765–1775 (2023), 10.1038/s41587-023-01747-2.
14. M. Eiraku *et al.*, Self-organizing optic-cup morphogenesis in three-dimensional culture. *Nature* **472**, 51–56 (2011).
15. X. Zhong *et al.*, Generation of three-dimensional retinal tissue with functional photoreceptors from human iPSCs. *Nat. Commun.* **5**, 4047 (2014).
16. A. Sridhar *et al.*, Single-cell transcriptomic comparison of human fetal retina, hPSC-derived retinal organoids, and long-term retinal cultures. *Cell Rep.* **30**, 1644–1659.e1644 (2020).
17. H. Liu *et al.*, Human embryonic stem cell-derived organoid retinoblastoma reveals a cancerous origin. *Proc. Natl. Acad. Sci. U.S.A.* **117**, 33628–33638 (2020).
18. B. Dorgau *et al.*, Human retinal organoids provide a suitable tool for toxicological investigations: A comprehensive validation using drugs and compounds affecting the retina. *Stem Cells Transl. Med.* **11**, 159–177 (2022).
19. J. Lakowski *et al.*, Isolation of human photoreceptor precursors via a cell surface marker panel from stem cell–derived retinal organoids and fetal retinae. *Stem Cells* **36**, 709–722 (2018).
20. R. A. Pearson *et al.*, Restoration of vision after transplantation of photoreceptors. *Nature* **485**, 99–103 (2012).
21. B. T. McLelland *et al.*, Transplanted hESC-derived retina organoid sheets differentiate, integrate, and improve visual function in retinal degenerate rats. *Invest. Ophthalmol. Vis. Sci.* **59**, 2586–2603 (2018).
22. J. Assawachananont *et al.*, Transplantation of embryonic and induced pluripotent stem cell–derived 3D retinal sheets into retinal degenerative mice. *Stem Cell Rep.* **2**, 662–674 (2014).
23. E. E. Capowski *et al.*, Reproducibility and staging of 3D human retinal organoids across multiple pluripotent stem cell lines. *Development* **146**, dev171686 (2019).
24. P. Ovando-Roche *et al.*, Use of bioreactors for culturing human retinal organoids improves photoreceptor yields. *Stem Cell Res. Ther* **9**, 156 (2018).
25. K. J. Wahlin *et al.*, Photoreceptor outer segment-like structures in long-term 3D retinas from human pluripotent stem cells. *Sci. Rep.* **7**, 766 (2017).
26. B. A. Tucker *et al.*, Patient-specific iPSC-derived photoreceptor precursor cells as a means to investigate retinitis pigmentosa. *Elife* **2**, e00824 (2013).
27. J. A. Cooke *et al.*, Propensity of patient-derived iPSCs for retinal differentiation: Implications for autologous cell replacement. *Stem Cells Transl. Med.* **12**, 365–378 (2023).
28. K. J. Wahlin *et al.*, CRISPR generated SIX6 and POU4F2 reporters allow identification of brain and optic transcriptional differences in human PSC-derived organoids. *Front Cell Dev. Biol.* **9**, 764725 (2021).
29. J. Toy, O. H. Sundin, Expression of the optx2 homeobox gene during mouse development. *Mech. Dev.* **83**, 183–186 (1999).
30. A. Kuwahara *et al.*, Generation of a ciliary margin-like stem cell niche from self-organizing human retinal tissue. *Nat. Commun.* **6**, 6286 (2015).
31. T. M. LaVaute *et al.*, Regulation of neural specification from human embryonic stem cells by BMP and FGF. *Stem Cells* **27**, 1741–1749 (2009).
32. M. T. Pankratz *et al.*, Directed neural differentiation of human embryonic stem cells via an obligated primitive anterior stage. *Stem Cells* **25**, 1511–1520 (2007).
33. J. Meyer, C. Zhang, Data from "A highly reproducible and efficient method for retinal organoid differentiation from human pluripotent stem cells". GEO Dataset. https://www.ncbi.nlm.nih.gov/geo/query/acc.cgi?acc=GSE254830. Deposited 1 February 2024.
34. B. L. Finlay, The developing and evolving retina: Using time to organize form. *Brain Res.* **1192**, 5–16 (2008).
35. F. J. Livesey, C. L. Cepko, Vertebrate neural cell-fate determination: Lessons from the retina. *Nat. Rev. Neurosci.* **2**, 109–118 (2001).
36. R. F. Leung *et al.*, Genetic regulation of vertebrate forebrain development by homeobox genes. *Front Neurosci.* **16**, 843794 (2022).
37. V. M. Sluch *et al.*, Enhanced stem cell differentiation and immunopurification of genome engineered human retinal ganglion cells. *Stem Cells Transl. Med.* **6**, 1972–1986 (2017).
38. C. M. Fligor, K. C. Huang, S. S. Lavekar, K. B. VanderWall, J. S. Meyer, Differentiation of retinal organoids from human pluripotent stem cells. *Methods Cell Biol.* **159**, 279–302 (2020).
39. S. K. Ohlemacher, C. L. Iglesias, A. Sridhar, D. M. Gamm, J. S. Meyer, Generation of highly enriched populations of optic vesicle–like retinal cells from human pluripotent stem cells. *Curr. Protoc. Stem Cell Biol.* **32**, 1h.8.1–1h.8.20 (2015).
40. J. Eintracht, P. Harding, D. Lima Cunha, M. Moosajee, Efficient embryoid-based method to improve generation of optic vesicles from human induced pluripotent stem cells. *F1000Res* **11**, 324 (2022).
41. S. Decembrini, S. Hoehnel, N. Brandenberg, Y. Arsenijevic, M. P. Lutolf, Hydrogel-based milliwell arrays for standardized and scalable retinal organoid cultures. *Sci. Rep.* **10**, 10275 (2020).
42. H. Döpper *et al.*, Differentiation protocol for 3D retinal organoids, immunostaining and signal quantitation. *Curr. Protoc. Stem Cell Biol.* **55**, e120 (2020).
43. A. L. Ludwig *et al.*, Re-formation of synaptic connectivity in dissociated human stem cell-derived retinal organoid cultures. *Proc. Natl. Acad. Sci. U.S.A.* **120**, e2213418120 (2023).
44. C. Gomes *et al.*, Astrocytes modulate neurodegenerative phenotypes associated with glaucoma in OPTN(E50K) human stem cell-derived retinal ganglion cells. *Stem Cell Rep.* **17**, 1636–1649 (2022).
45. K. B. VanderWall *et al.*, Astrocytes regulate the development and maturation of retinal ganglion cells derived from human pluripotent stem cells. *Stem Cell Rep.* **12**, 201–212 (2019).
46. X. Duan *et al.*, Cadherin combinations recruit dendrites of distinct retinal neurons to a shared interneuronal scaffold. *Neuron* **99**, 1145–1154.e1146 (2018).
47. J. Rainger *et al.*, Monoallelic and biallelic mutations in MAB21L2 cause a spectrum of major eye malformations. *Am. J. Hum. Genet.* **94**, 915–923 (2014).
48. H. Sun, J. Nathans, Stargardt's ABCR is localized to the disc membrane of retinal rod outer segments. *Nat. Genet.* **17**, 15–16 (1997).
49. M. Maqueda, J. L. Mosquera, J. García-Arumí, A. Veiga, A. Duarri, Repopulation of decellularized retinas with hiPSC-derived retinal pigment epithelial and ocular progenitor cells shows cell engraftment, organization and differentiation. *Biomaterials* **276**, 121049 (2021).
50. A. Sridhar, S. K. Ohlemacher, K. B. Langer, J. S. Meyer, Robust differentiation of mRNA-reprogrammed human induced pluripotent stem cells toward a retinal lineage. *Stem Cells Transl. Med.* **5**, 417–426 (2016).
51. A. Sridhar, M. M. Steward, J. S. Meyer, Nonxenogeneic growth and retinal differentiation of human induced pluripotent stem cells. *Stem Cells Transl. Med.* **2**, 255–264 (2013).
52. E. L. West *et al.*, Antioxidant and lipid supplementation improve the development of photoreceptor outer segments in pluripotent stem cell-derived retinal organoids. *Stem Cell Rep.* **17**, 775–788 (2022).
53. C. M. Fligor *et al.*, Extension of retinofugal projections in an assembled model of human pluripotent stem cell-derived organoids. *Stem Cell Rep.* **16**, 2228–2241 (2021).
54. S. S. Lavekar *et al.*, Development of a three-dimensional organoid model to explore early retinal phenotypes associated with Alzheimer's disease. *Sci. Rep.* **13**, 13827 (2023).
55. K. J. Livak, T. D. Schmittgen, Analysis of relative gene expression data using real-time quantitative PCR and the 2(-Delta Delta C(T)) Method. *Methods* **25**, 402–408 (2001).